HHS Public Access

Author manuscript

Cell Rep. Author manuscript; available in PMC 2026 February 13.

Published in final edited form as:

Cell Rep. 2025 December 23; 44(12): 116624. doi:10.1016/j.celrep.2025.116624.

Spatial and single-cell transcriptomics reveal the reorganization of cerebellar microglia with aging

Andy P. Tsai[1,2,11], **Douglas E. Henze**[3,11], **Eduardo Ramirez Lopez**[1,2], **James Haberberger**[4], **Chuanpeng Dong**[5], **Nannan Lu**[1,2], **Micaiah Atkins**[1,2,6], **Emma K. Costa**[1,2,7], **Amelia Farinas**[1,2,7], **Hamilton Se-Hwee Oh**[1,2], **Patricia Moran-Losada**[1,2], **Yann Le Guen**[8], **Alina Isakova**[4], **Stephen R. Quake**[3,9,10,*], **Tony Wyss-Coray**[1,2,4,12,*]

[1]Department of Neurology and Neurological Sciences, Stanford University School of Medicine, Stanford, CA, USA

[2]Wu Tsai Neurosciences Institute, Stanford University, Stanford, CA, USA

[3]Department of Bioengineering, Stanford University, Stanford, CA, USA

[4]The Phil and Penny Knight Initiative for Brain Resilience, Stanford University, Stanford, CA, USA

[5]Department of Genetics, Yale University School of Medicine, New Haven, CT, USA

[6]State University of New York Downstate Health Science University, College of Medicine, Brooklyn, NY, USA

[7]Neurosciences Interdepartmental Program, Stanford University School of Medicine, Stanford, CA, USA

[8]Quantitative Sciences Unit, Department of Medicine, Stanford University, Stanford, CA, USA

[9]Department of Applied Physics, Stanford University, Stanford, CA, USA

[10]Chan Zuckerberg Initiative, Redwood City, CA, USA

[11]These authors contributed equally

[12]Lead contact

SUMMARY

The cerebellum, essential for motor coordination and increasingly recognized for its role in cognition, is typically considered more resilient to aging and largely spared from hallmark Alzheimer's disease (AD) pathology. However, transcriptomic analyses across fifteen mouse brain regions revealed that the cerebellum undergoes some of the earliest and most pronounced

*Correspondence: steve@quake-lab.org (S.R.Q.), twc@stanford.edu (T.W.-C.).

AUTHOR CONTRIBUTIONS

A.P.T. and D.E.H. conceptualized and designed the experiments. A.P.T., D.E.H., E.R.L., N.L., and M.A. conducted the experiments and collected the data. A.P.T., D.E.H., E.R.L., J.H., and C.D. analyzed the data. A.P.T., D.E.H., E.R.L., J.H., C.D., E.K.C., A.F., H.S.-H.O., P.M.-L., Y.L.G., A.I., S.R.Q., and T.W.-C. discussed and interpreted the data. A.P.T., D.E.H., E.R.L., J.H., and C.D. designed the figures. A.P.T. wrote the manuscript. D.E.H., S.R.Q., and T.W.-C. edited the manuscript. A.P.T., D.E.H., S.R.Q., and T.W.-C. supervised, directed, and managed the study. All authors discussed the results and commented on the manuscript.

DECLARATION OF INTERESTS

The authors declare no competing interests.

age-related changes. To investigate cerebellar aging, we applied single-nucleus RNA sequencing (RNA-seq), microglial bulk RNA-seq, and multiplexed error-robust fluorescence *in situ* hybridization (MERFISH)-based spatial transcriptomics. Microglia showed the most prominent changes, including elevated expression of a neuroprotective signature and reduced expression of a lipid-droplet-accumulating signature compared to hippocampal microglia. Spatial analyses further revealed that aged cerebellar microglia were positioned in close proximity to granule cells. Utilizing this relationship, we identified a proximity-dependent transcriptional state defined by the neuron-associated microglial signature. This signature reveals a region-specific microglial adaptation, highlighting cerebellar reorganization with age and potential resilience to AD.

In brief

Tsai et al. show that cerebellar microglia undergo distinct molecular and spatial changes during aging. Integrated single-nucleus and spatial transcriptomics identify a neuron-associated microglial state linked to increased microglia-neuron proximity and neuroprotective gene expression, revealing region-specific microglial adaptation in the aged cerebellum.

Graphical abstract

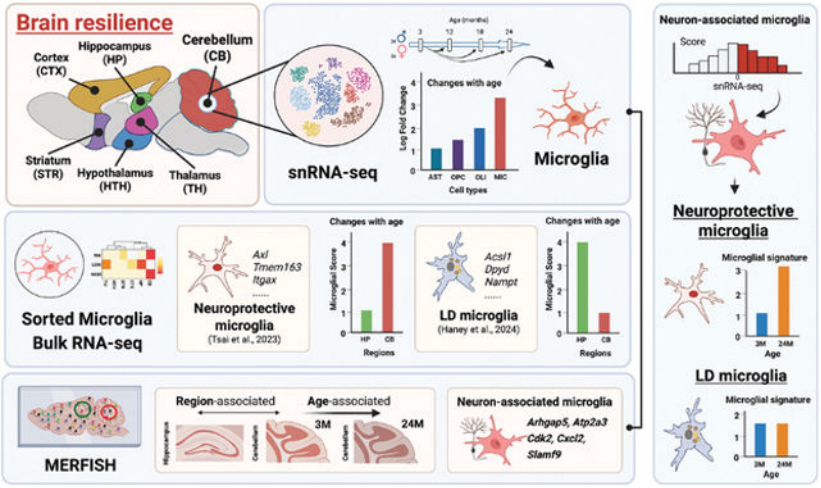

INTRODUCTION

Aging is a primary driver of organ dysfunction[1] and the leading risk factor for neurological disorders.[2] Understanding the mechanisms of brain aging is essential for developing strategies to combat age-related neurodegeneration, ultimately enhancing quality of life and extending cognitive health. This process is complex, as different brain regions age at varying rates, with some areas showing greater vulnerability to age-related changes.[3–6] The cerebellum, which contains approximately 70%–80% of the brain's neurons[7] and is critical for motor coordination, sensory integration, and cognitive processing,[8,9] is among the regions most affected by aging, exhibiting structural and functional decline.[3] This deterioration contributes to an increased risk of falls, driven by impairments in balance, motor function, and fine motor skills.

Despite these vulnerabilities, the cerebellum demonstrates remarkable resilience to Alzheimer's disease (AD) pathology.[10,11] Amyloid plaques are largely absent during early stages, and dystrophic neurites are rarely observed throughout the disease progression.[12] This resilience raises intriguing questions about the molecular and cellular mechanisms that confer protection against AD pathologies in the cerebellum. However, the lack of detailed studies on glial cell involvement in cerebellar aging has limited our understanding of age-related adaptations in this brain region, even though microglia display high expression of AD risk genes.[13,14]

Cerebellar microglia are essential for maintaining neuronal homeostasis, with their high basal clearance activity likely mitigating cellular debris accumulation and preserving brain integrity.[15] This activity, distinct from other brain regions, may drive a unique microglia-mediated neuronal attrition, providing an adaptive mechanism to sustain cerebellar function during the natural decline in neuronal numbers observed in late adolescence.[16] Despite their importance, glial cell gene expression and spatial organization, including that of microglia, remain poorly characterized during healthy aging, leaving a significant gap in our understanding of how the cerebellum adapts to age-related changes. The cerebellum's evolutionary conservation across vertebrates, coupled with its pronounced age-related changes, positions it as a unique model for studying brain aging.[17] However, it remains unclear whether molecular alterations in this highly conserved region can be leveraged to identify signatures of brain aging. Addressing these gaps is critical for uncovering the mechanisms underlying cerebellar resilience to AD and understanding their broader role in age-related changes across the brain.

RESULTS

Distinct transcriptional aging patterns in cerebellar cells

Cerebellar aging remains poorly understood, with limited insight into its molecular alterations. To address this, we isolated and analyzed the transcriptome of nuclei from the cerebellum of two female and two male mice each at 3, 12, 18, and 24 months of age. NeuN-negative and NeuN-positive nuclei were sorted to enrich for glial cell types, followed by single-nucleus RNA sequencing (snRNA-seq) of 87,677 individual nuclei. Uniform manifold approximation and projection (UMAP) analysis identified 16 transcriptionally distinct clusters, each representing a major cerebellar cell type (Figure 1A). These clusters were annotated based on the expression of well-established molecular markers specific to cerebellar cells[18] (Figure 1B). To characterize cell-type-specific transcriptional aging signatures, we performed differential expression analysis of snRNA-seq data, comparing the 3-month-old group to older age groups (12, 18, and 24 months old). This analysis revealed distinct trajectories of differentially expressed genes (DEGs) for each cell type over time. Notably, microglia exhibited the most pronounced changes among the various cell types, particularly in the oldest cohort of 24-month-old mice, as shown by the average log fold change of the top ten upregulated DEGs (Figure 1C). To further identify aging-associated genes, we applied the Mfuzz algorithm to cluster pseudo-bulk snRNA-seq data, which uncovered nine distinct gene expression trajectories across time points (Figure 1D). Genes within clusters 1 and 7 demonstrated a strong correlation with aging, showing increasing

expression levels with age (Figure 1E). Remarkably, these age-associated genes were predominantly expressed in microglia (Figure 1F), suggesting this cell type as the most transcriptionally responsive to aging. These findings highlight distinct, cell-type-specific transcriptional adaptations within the cerebellum during aging, with microglia emerging as prominent responders to age-related functional changes.

Regional and age-associated transcriptional signatures of microglia

Acknowledging that different regions age at varying rates,[3] we investigate whether cerebellar microglia exhibit distinct transcriptional signatures compared to other brain regions. To address this, we examined the cortex (CTX), hippocampus (HP), thalamus (TH), hypothalamus (HTH), and striatum (STR). Microglia were isolated from these six regions of 1-, 3-, and 22-month-old male mice ($n = 6$ per group), and transcriptomes were quantified using bulk RNA-seq (Figure 2A). Principal-component analysis (PCA) revealed a major effect of age on gene expression across brain regions, with principal component 1 (PC1) scores increasing progressively with age. Notably, PC1 scores were highest in the cerebellum and lowest in the HP and CTX, suggesting a unique transcriptional trajectory in cerebellar microglia during aging (Figures 2B and 2C). Weighted gene co-expression network analysis (WGCNA) identified four key gene modules (microglia M4, M9, M10, and M12) strongly associated with either age or brain region (Figure 2D). Aging was linked to increased expression of the M4 and M12 modules and decreased expression of the M9 and M10 modules. These trends were most pronounced in cerebellar microglia, which exhibited the highest M4 module scores and the lowest M9 and M10 scores. Conversely, aged hippocampal microglia demonstrated higher M9 and M10 scores compared to their cerebellar counterparts (Figure 2E). Gene Ontology (GO) enrichment analysis revealed that the M4 module was enriched for the type I interferon signaling pathway and cytokine-mediated signaling pathway, while the M12 module was linked to small GTPase-mediated signal transduction. Receptor-mediated endocytosis was associated with the M9 module, and the M10 module was enriched for regulation of autophagy (Figure 2F). These biological processes are critically linked to the immune response, cellular signaling, and homeostasis. For instance, type I interferon signaling (M4) plays a vital role in immune regulation, while autophagy (M10) maintains cellular integrity. In addition, small GTPase signaling (M12) and receptor-mediated endocytosis (M9) may influence cell communication and internalization, providing insights into molecular mechanisms of microglial aging and highlighting potential therapeutic targets for modulating these processes. To further identify microglial genes affected by age and region, we performed differential gene expression analysis on sorted microglia, comparing the cerebellum and HP, as well as 22- and 3-month-old groups. Genes that were differentially expressed in both comparisons, including *Axl*, *Apoe*, *C4b*, *Lpl*, *Spp1*, *Hcar2*, and *Stat1*, show distinct expression patterns across brain regions and age groups (Figure 2G). To better characterize microglial functional states, previously published transcriptional signatures were used to compute distinct microglial scores based on the average expression of each gene set (STAR Methods). These included signatures of neuroprotective microglia[19] (Figure 2H), lipid-droplet (LD)-accumulating microglia[20] (Figure 2I), senescence and anti-senescence,[21,22] disease-associated microglia,[23] and activation[24] (Figures S1A–S1D). The neuroprotective microglial signature, previously described and linked to the amyloid plaque response and the protective effects of the

phospholipase C-gamma 2 (PLCG2) P522R variant, was highly expressed in aged cerebellar microglia (Figure 2H). In contrast, the LD-accumulating microglial signature, associated with lipid metabolism, microglial dysfunction, and AD pathology, showed significantly higher expression in the CTX and HP (Figure 2I). These findings suggest that regional differences in the expression of the LD accumulation microglial signature, a feature linked to neurotoxicity and neuroinflammation, may underlie distinct susceptibilities to aging and neurodegeneration.

Increased microglial proximity to granule cells defines the aged cerebellum

To investigate the distinct transcriptional response of cerebellar microglia during aging, we estimated their spatial proximity to neighboring cells, including neurons, and compared these patterns to hippocampal microglia. Multiplexed error-robust fluorescence *in situ* hybridization (MERFISH) was applied to quantify spatial organizations and transcriptional signatures within the cellular architecture of the aging cerebellum and HP. A parasagittal view of the mouse cerebellar and hippocampal layers is shown in Figure 3A. MERFISH imaging was performed on sagittal sections of six mouse brains per sex, including both young (3-month-old) and aged (24-month-old) mice, using a panel of 500 genes selected for their relevance to aging, neuroinflammation, cellular stress, and cell-type specificity across brain regions. Cell types were annotated by integrating data with the Allen Brain Cell Atlas.[25] MERFISH images of the identified brain regions, including the basal ganglia, cerebellum, CTX, HP, HTH, TH, and midbrain, pons, and medulla (MPM) region, are colored and shown in Figure S2A. The dataset contained 991,315 cells spanning 38 major cell classes across these 7 identified brain regions (Figure S2B), with microglial distribution quantified (Figure S2C). To explore aging-associated spatial reorganization, we analyzed microglial cellular neighborhoods, defined by a radial distance of 30 μm in the cerebellum and HP. Representative images with cell-type labeling are shown in Figure 3B. In the aged cerebellum, compared to the young, we observed increased granule-cell-associated microglia (Figure 3C). In contrast, the aged HP exhibited increased microglia with other cells in the microglial neighborhoods (Figure 3D). MERFISH images of the cerebellum and HP from both 3-month-old and 24-month-old mice revealed distinct spatial patterns of microglial organization during aging (Figure 3E). We further quantified the percentage of microglia in the white matter area, granule layer, and molecular layer of the cerebellum, identifying a significant increase in microglial density with the granule layer of aged mice across different cerebellar layers at each age, including those analyzed using MERFISH images. (Figure 3F). This finding was validated by immunofluorescence staining, which showed increased coverage of IBA1-positive microglia in the GABRA6-positive granule cell area of the cerebellum compared to 3-month-old young mice. (Figures 3G and S2D). To investigate the changes in transcriptomic signatures associated with spatial organization, we analyzed DEGs in microglia from the granule layer of aged mice compared to other cellular layers. Notably, microglia in the granule cell layer of aged mice show increased expression of genes involved in synaptic signaling, immune response, and cell cycle regulation, including *Cbln1*, *Cdk2*, *Cxcl2*, *Slamf9*, and *Adcy1* (Figure 3H), suggesting a spatially distinct and adaptive microglial state in the aged cerebellum.

Cerebellar microglial states are associated with spatial proximity to granule cells

In aged mice, genes upregulated in granule layer microglia, including those involved in synaptic signaling and cell cycle regulation, suggest an adaptive microglial state linked to cerebellar aging. To investigate whether proximity to granule cells contributes to distinct microglial states, we examined the relationship between spatial organization and microglial gene expression, focusing on genes enriched in microglia located near granule cells (Figure 4A). The microglial cell cycle signature includes genes typically induced in response to stress, injury, or debris clearance. We quantified the expression of this signature using a *Z* scored average and assessed its association with distance to granule cells in both the cerebellum and HP. Notably, the expression of the microglial cell cycle signature was strongly associated with proximity to granule cells in the aged cerebellum (Figure 4B), whereas no such association was observed in the HP (Figure 4C). To further investigate proximity-driven microglial states, we used MERFISH to identify genes with elevated expression in microglia near cerebellar granule cells and defined a new neuron-associated microglial signature. This gene set captures a unique transcriptional profile associated with spatial proximity to granule cells and their local environment. Microglia expressing this signature at high levels were described as possessing a neuron-associated microglial state. Our analysis revealed that this neuron-associated microglial state varied across brain regions and was most pronounced within 40 μm of granule cells, with the highest average expression (*Z* scored) observed in aged cerebellar microglia (Figures 4D and 4E). We visualized the expression of genes contributing to the neuron-associated microglial signature, including *Arhgap5*, *Atp2a3*, *Cdk2*, *Cxcl2*, and *Slamf9* in the cerebellum (Figures S3A–S3J) and HP (Figures S4A–S4J). The specificity of the neuron-associated microglial state was evident in its gene expression patterns across individual glial cell types located within 30 μm of the granule cells in the aged cerebellum and HP (Figure S5A). Supporting its validity, the neuron-associated microglial signature showed significantly higher expression in aged cerebellar microglia compared to young cerebellar microglia and other glial cell types in the aged cerebellum (Figure S5B). We further quantified this signature across five brain regions (Figure S5C), three cerebellar layers (Figure S5D), and sorted microglia bulk RNA-seq data from six regions across three ages (Figure S5E). These analyses demonstrated the utility of this novel neuron-associated microglial signature in identifying regionally distinct microglial states and capturing the influence of spatial organization on transcriptional changes in microglia during aging. Although originally identified in aged cerebellar microglia, the signature serves as a versatile tool for characterizing the microglial state across diverse brain regions.

Age-associated adaptations in neuron-associated microglia

To investigate how aging affects neuron-associated microglia, we examined the morphological and transcriptional adaptations of microglia in the cerebellum. In aged mice, cerebellar microglia exhibited increased proximity to granule cells and reduced arbor complexity compared to young brains (Figures 5A and 5B). In the young cerebellum, Spearman correlation analysis revealed that greater distance from the granule cells was associated with increased microglial complexity, including increased branching, larger cell area, and higher fractal dimension. In contrast, these spatial correlations were attenuated in the aged cerebellum, where proximity to granule cells was instead positively correlated

with features indicative of cellular compactness, such as increased cell circularity, solidity, and convex hull circularity (Figure 5C). These findings suggest that aging disrupts the spatial regulation of microglial morphology, favoring a shift toward a more compact cellular architecture near granule cells. To characterize this spatially distinct population in an unbiased manner, we examined neuron-associated microglial signature expression in snRNA-seq data. We defined neuron-associated microglia as those displaying a positive score of the signature expression (Figure 5D). Differential gene expression analysis of this microglial population revealed age-associated transcriptional remodeling, including upregulation of genes involved in cell migration and morphology (*Arhgap5*) as well as cytoskeletal organization and vesicular trafficking (*Myo5a*), alongside down-regulation of *Itga9*, a gene linked to microglial homeostasis and activity (Figure 5E). Neuron-associated microglia in the aged cerebellum exhibited significantly elevated expression of the neuroprotective microglial signature (Figure 5F), while expression of the LD-accumulating microglial signature remained unchanged (Figure 5G). These findings suggest that aging may selectively promote neuroprotective transcriptional states in neuron-associated microglia without concurrently inducing LD-associated pathological signatures in mice.

DISCUSSION

Age is the greatest known risk factor for AD, yet the cellular mechanisms that confer resilience versus vulnerability during brain aging remain poorly understood. Similar to distinct aging trajectories observed across organs,[26] different brain regions exhibit specific transcriptional changes with age, with the cerebellum among the most transcriptionally responsive.[3,15] Given its strong evolutionary conservation across species and its emerging role in cognitive function,[17,27] the cerebellum represents a powerful model for investigating the molecular and cellular adaptations underlying brain aging and cognitive decline. However, detailed single-cell resolution data on glial cells and analyses of cerebellar glial adaptations have been limited prior to this study.[28]

By integrating cerebellar snRNA-seq, sorted microglia RNA-seq, and MERFISH-based spatial transcriptomics, we identified cerebellar microglia as the most transcriptionally responsive cell types during aging, adopting neuroprotective immune programs associated with brain resilience. These adaptations were accompanied by the upregulation of immune activation genes, including *Axl*, *Lilrb4a*, *Cybb*, *Apoe*, *Lpl*, *Lgals3*, and *Hcar2*, paralleling the elevated neuroprotective microglial signature previously associated with microglia harboring an AD-protective PLCG2 variant.[19,29] These transcriptional signatures likely enhance the capacity of cerebellar microglia to facilitate debris clearance and reduce neuronal stress, thereby promoting resilience. Notably, these changes occurred without inducing a pathological LD accumulation-related microglial state. In contrast, hippocampal microglia exhibited higher expression of LD-related genes, including *Acsl1*, *Nampt*, *Dpyd*, and *Cd163*,[20,30] which have been implicated in neurotoxicity, neuroinflammation, and vulnerability to neurodegeneration.[20] This divergence underscores region-specific microglial adaptations, with cerebellar microglia engaging an immune-neuron axis to support local resilience, while hippocampal microglia maintain a homeostatic state that may be less effective in mitigating age-related stress.

Spatial transcriptomics revealed a significant reorganization of cerebellar microglia during aging, marked by increased proximity to granule cells. This spatial shift suggests that microglia in the aged cerebellum increasingly engage with granule cells, potentially maintaining local tissue homeostasis. To further explore this phenomenon, we identified a neuron-associated microglial signature based on genes enriched in microglia located near granule cells. Analysis of signature expression revealed the emergence of a proximity-dependent transcriptional program selectively enriched in aged cerebellar microglia, supporting the concept that local neuron-microglia interactions remodel microglial aging trajectories. Although specialized and adapted to different demands, granule cells are present in both the cerebellum and HP[18,31] and have been implicated in cognitive impairments associated with aging.[32,33] The granule-cell-rich architecture of the cerebellum likely facilitates cell-type-specific interactions, enabling microglia to respond dynamically to age-related changes in their local environment.

Within neuron-associated microglia, aging was associated with increased expression of *Arhgap15* and *Myo5a*, genes involved in cell migration, morphology, cytoskeletal remodeling, and vesicular transport, with links to cerebellar function and ataxia,[34,35] alongside decreased expression of *Itga9*, a key integrin adhesion receptor that plays a role in mediating cell-cell and cell-matrix adhesion[36] and modulates tau neurotoxicity in AD *Drosophila* models.[37] These transcriptional adaptations were accompanied by elevated expression of the neuroprotective microglial signature without a corresponding increased expression of the LD-accumulating microglial signature, reinforcing the idea that spatially organized resilience-associated programs may actively sustain neuronal health during aging.

The elevated expression of the neuroprotective microglial signature in cerebellar microglia suggests their role in preserving neuronal integrity, as the associated genes have been previously linked to neuroprotective responses to amyloid plaques.[19] In addition, the lower expression of the LD-accumulating microglial signature in the cerebellum compared to the HP reflects a reduced susceptibility to LD accumulation, a process implicated in neurodegeneration, particularly in APOE4 carriers.[20] These region-specific differences highlight the enhanced ability of the cerebellum to mitigate age-related stressors and its relative resilience compared to other brain regions.

In conclusion, this study reveals a region-specific aging response in cerebellar microglia, suggesting a new conceptual model of brain aging in which targeted neuron-associated microglial responses, rather than generalized immune activation, are essential for maintaining regional brain integrity. These findings provide insight into potential protective mechanisms in the aging brain and suggest that targeted modulation of microglial function may support brain health and resilience to neurodegeneration in vulnerable brain regions.

Limitations of the study

Although this study is observational in nature and limits direct causal inference, the genes comprising the neuroprotective and LD-accumulating microglial signatures have been functionally validated in our previous studies, supporting their biological relevance.[19,20] While single-cell RNA-seq, sorted microglia RNA-seq, and spatial transcriptomics provide high-resolution profiling, functional validation of the neuron-associated microglial signature,

particularly its connection to brain resilience, will require new experimental approaches capable of selectively manipulating microglia within spatially defined regions.

Future studies should aim to develop strategies to selectively enhance the neuron-associated microglial program in specific brain regions and determine whether reinforcing these protective states preserves brain function without disrupting region-specific homeostasis. Targeting spatially organized microglial adaptations represents a promising therapeutic avenue for promoting resilience during brain aging and in AD.

RESOURCE AVAILABILITY

Lead contact

Further information and requests for resources and reagents should be directed to and will be fulfilled by the lead contact, Tony Wyss-Coray (twc@stanford.edu).

Materials availability

This study did not generate new unique reagents. Materials generated in this study will be available upon completion of a materials transfer agreement (MTA).

Data and code availability

- Sequencing data are available through Gene Expression Omnibus (GEO): GSE290806.
- Code used to analyze the datasets is available on GitHub at https://github.com/doughenze/Aging_CB.
- Any additional information required to reanalyze the data reported in this paper is available from the lead contact upon request.

STAR★METHODS

EXPERIMENTAL MODEL AND STUDY PARTICIPANT DETAILS

Mice: C57BL/6J male and female mice (stock # 000664) were purchased from Jackson Laboratories. Up to five mice were housed per cage under specific-pathogen-free conditions in the Wu-Tsai Neurosciences Research Institute Veterinary Service Center at Stanford University School of Medicine. The colony room was maintained on a 12:12 h light/dark cycle with food and water provided *ad libitum*. Mice were euthanized by perfusion with ice-cold phosphate-buffered saline (PBS) following full anesthetization with Avertin (125–250 mg/kg intraperitoneal injection). All animal care and experimental procedures complied with the Guide for the Care and Use of Laboratory Animals of the National Institutes of Health and were approved by Stanford University's Administrative Panel on Laboratory Animal Care (APLAC).

METHOD DETAILS

Nuclei isolation and fluorescence-activated cell sorting (FACS): Nuclei were isolated from the fresh-frozen cerebellar region of the left hemisphere of mice using Dounce

homogenizers (Sigma-Aldrich, St. Louis, USA #D8938), and the Nuclei EZ Prep Kit (Sigma-Aldrich #Nuc101–1KT) according to previously published methods.[19] The nuclei were then centrifuged at 300 g for 10 min at 4°C and resuspended in 50 μL of FACS buffer (1% BSA, 1x PBS; sterile filtered) containing 2 U/ml of Recombinant RNase Inhibitor (Takara #2313B) and anti-CD16/CD32 Fc block (BD Biosciences #553142). After incubation for 5-min, 50 μL of an antibody cocktail in FACS buffer containing 1 μL of NeuN antibody (Abcam #ab190565) and Recombinant RNase Inhibitor was added.

Samples were incubated with staining antibodies on ice for 30 min with gentle shaking, followed by centrifugation at 300*g* for 10 min at 4°C. Nuclei were resuspended in 500 μL of FACS buffer containing Recombinant RNase Inhibitor and 1 μL of Hoechst 33342 was added. NeuN-positive and NeuN-negative nuclei were sorted separately into 1.5 mL DNA LoBind tubes containing 1 mL of final buffer (200 μL UltraPure BSA, Thermo #AM2618, 800 μL PBS, and 5 μL Protector RNase Inhibitor). A total of 50,000 single nuclei were sorted per sample. Nuclei concentrations were adjusted to ~1 million nuclei/ml.

Chromium 10X library generation and illumina sequencing: Chromium 10X library generation and Illumina sequencing were conducted following previously published methods.[19] Reagents for the Chromium Single Cell 3′ Library & Gel Bead Kit v3.1 (10X Genomics, Pleasanton, USA) were thawed and prepared following the manufacturer's protocol. The nuclei/master mix solution was adjusted to target 10,000 nuclei per sample (5,000 from male mice and 5,000 from female mice) and loaded onto a standard Chromium Controller (10X Genomics) as instructed. All reactions, including library construction using the Chromium Single Cell 3′ Library Construction Kit v3, were performed according to the manufacturer's protocol using the recommended reagents, consumables, and instruments. Quality control for cDNA and libraries was conducted using a Bioanalyzer (Agilent, Santa Clara, USA) at the Stanford Protein and Nucleic Acid Facility. Illumina sequencing of the 10X snRNA-seq libraries was performed by Novogene Co. Inc. (Sacramento, USA). Multiplexed libraries were sequenced using 2 × 150-bp paired-end reads in a single S4 lane on an Illumina NovaSeq S4 (Illumina, San Diego, USA), targeting 100 million reads per library. Base-calling, demultiplexing, and FASTQ file generation were performed for further data analysis.

QUANTIFICATION AND STATISTICAL ANALYSIS

Single-nuclei RNA sequencing (snRNA-seq) analysis: The snRNA-seq reads were aligned to the mouse genome reference (mm10) using CellRanger (v7.1.0). Downstream analysis, including quality control (QC), cell clustering, and differential gene detection, was performed using the Seurat package. Specific QC criteria were applied as follows: (1) cells with less than 200 or more than 5000 detected features, or with more than 5% mitochondrial UMI counts, were removed; (2) integration was performed using LogNormalize on the top 3000 highly variable features, with default settings for other parameters; (3) clustering resolution was set to 0.6. UMAP was used for dimensionality reduction, and clusters were manually annotated based on canonical marker gene expression. These markers include *Gabra6* for granule cells (Granule), *Mog* and *Mobp* for oligodendrocytes (Oligo), *Aqp4* for astrocytes, *Col1a1* for fibroblasts, *Lypd6* for molecular layer interneurons (MLIs), *Gdf10* for

Bergmann glia (Bergmann), *Ttr* for choroid plexus (Choroid), *Pecam1* for endothelial cells (Endo), *Kcnj8* for endothelial and mural cells (Endo.Mural), *Klhl1* and *Lgi2* for Golgi cells (Golgi), *Plcg2* and *P2ry12* for microglia, *Pdgfra* and *Olig2* for oligodendrocyte progenitor cells (OPCs), *Gad1* and *Gad2* for Purkinje layer interneurons (PLIs), *Ppp1r17* for Purkinje cells (Purkinje), *Eomes* for unipolar brush cells (UBCs), and *Mrc1* for border associated macrophages (BAM). Differentially expressed genes between cell types and conditions were identified using Seurat's FindMarkers function.

Time-dependent genes were clustered using the R package Mfuzz, which applies soft clustering using the fuzzy c-means algorithm. The data of snRNA-seq were aggregated into pseudo-bulk values as input for Mfuzz clustering. The number of clusters was set to 9, and the optimal fuzzifier coefficient (m) was determined using the 'mestimate' function.

Microglia isolation and bulk RNA-seq analysis: Microglia were isolated using ice-cold dounce homogenization, based on published methods.[38] After perfusing mice with PBS, six brain regions (hypothalamus, thalamus, hippocampus, striatum, cortex, cerebellum) were dissected, chopped, and homogenized in cold medium A (HBSS, 15 mM HEPES, 0.5% glucose, and 1:500 DNase I). The homogenate was filtered and centrifuged. Myelin was removed with MACS myelin removal beads (Miltenyi Biotech) and MACS buffer (1x PBS, 2 mM EDTA, 0.5% BSA), followed by cell resuspension in FACS buffer (1x PBS, 2 mM EDTA, 1% FBS, 25 mM HEPES) with FC blocking (CD16/CD32). Cells were stained with CD11b-FITC, CD45-BUV395, and CD206-PE-Cy7, then washed, centrifuged, and dead cells excluded with Sytox Blue (1:1000). 6,000 microglia were sorted into RLT lysis buffer (Qiagen) with 1% 2-mercaptoethanol (Sigma, M6250) and frozen at −80°C.

RNA was extracted with the RNeasy Plus Micro kit (Qiagen, 74034). cDNA and libraries were synthesized in-house using a modified Smart-seq2 protocol as previously described.[3,39,40] Amplified cDNA was prepared for library sequencing, including bead clean-up, tagmentation, and indexing. Libraries were purified and assessed for quality using a Bioanalyzer (Agilent), then sequenced with Next-seq 550 high-output kit systems (Illumina, 20024907, paired end, 2 × 75 bp depth).

Principal Component Analysis (PCA) was conducted using scikit-learn package in python using normalized bulk RNA-seq data. Weighted Gene Co-expression Network Analysis (WGCNA) was used to identify gene modules correlated with traits of interest from bulk RNA-seq data. Data were normalized and filtered to retain highly variable genes. A soft-thresholding power was selected to create a scale-free network, and a topological overlap matrix (TOM) was used to cluster genes, identifying co-expression modules. Module eigengenes, representing module expression profiles, were correlated with traits to find significant associations. Gene Ontology (GO) enrichment analysis was performed on significant modules, and hub genes were identified based on module connectivity.

Gene set signature scores were calculated from microglial bulk RNA-seq data by averaging the expression of selected genes associated with the biological process of interest followed by subtraction of the average expression for a reference set of genes. Normalized expression values were used to calculate an average score per sample. Boxplots were used to compare

scores across conditions. Data processing and visualizations were performed in Python using seaborn for boxplots. Neuroprotective microglia scores[19] were calculated by genes including *Axl*, *Cd9*, *Csf1r*, *Hif1a*, *Itgax*, *Tmem163*, *Apoe*, *Cybb*, *Lilr4b*, *Lgals3*; LD-accumulating microglia score[20,30] were calculated by genes including *Slc25a5*, *Npl*, *Angptl7*, *Pde2a*, *Ldhb*, *Cd63*, *Sepp1*, *Sdcbp*, *Adipor1*, *Rbbp4*, *Cndp2*, *Hsd17b4*, *Gpd11*, *Dazap2*, *Hnmpk*, *Rapsn*, *Cat*, *Kl*, *Nampt*, *Acsl1*, *Dpyd*, *Cd163*; senescence score were calculated by genes including *Ccl2*, *Tgfb1*, *Il1b*, *Mmp3*, *Ccl5*, *Cxcl10*, *Serpine1*, *Cdkn2a*, *Glb1*, *Tnf*, *Il6*, *Cdkn1a*; Anti-senescence score were calculated by genes including *Cdk4*, *Rb1*, *Cdk2*, *Lmnb1*, *Mki67*, *Cdk6*; DAM score[23,41] were calculated by genes including *Trem2*, *Apoe, Tyrobp*, *Itgax, Clec7a*, *Lpl*, *Cst7*, *Spp1*, *Axl, Cd9*; Activation score[24] were calculated by genes including *B2m*, *Trem2*, *Ccl2*, *Apoe*, *Axl*, *Itgax*, *Cd9*, *C1qc*, *Lyz2*, *Ctss*, and Neuron-associated microglia score were calculated by genes including *Cdk2*, *Cxcl2*, *Slamf9*, *Arhgap5*, *Atp2a3*.

MERFISH analysis: The annotated and pre-processed MERFISH data were obtained from Henze et al.[42] These data were used to analyze cell-cell interaction within the different brain regions at 3 and 24-month-old mice. As described previously,[43] cells were only analyzed if they had a subclass label-transfer confidence score greater than 0.8. For each cell type pair within each region at each age, we then determined the number of each cell type contacting them and compared the difference between young and old contact pairs against the difference in the null distributions for each age. The null distributions were generated by locally shifting the positions of the cell types to random locations and calculating the cell-cell contacts amongst them. To consider two cells in proximity to one another, we established a distance threshold of 30 μm. We generated the null distribution by randomly shifting local cell positions within each brain region and counting cell-cell proximal pairs over 1000 rounds of permutations. To determine differences in cell-cell contacts, we fitted the distribution of differences between data from 3- and 24-month-old mouse samples contacts to the normal distribution and calculated the *p*-value for the ratiometric change between the ages to determine differences in the probability of cell-cell interaction with age.

To then analyze the number of microglia within each region of the cerebellum we analyzed only the cells of the cerebellum and for microglia that were closer to a Purkinje cell than to a granule cell we classified them as being from the molecular layer. The remaining cells were then divided amongst being in the granule layer versus in the white matter if the microglia were within 30 μm of a granule neuron, and the remainder of the microglia were delineated as white matter originating.

We then computed scores from the normalized and log-transformed gene expression values using the score_genes function in Scanpy. The genes used to examine the expression of cell cycle signature (cell cycle score) include: '*Cdk4*','*Rb1*','*Cdk2*','*Lmnb1*','*Mki67*', and '*Cdk6*'. The genes used to examine the neuron-associated microglial signature (neuron-associated microglia score) include: '*Cdk2*', '*Cxcl2*', '*Slamf9*', '*Arhgap5*', and '*Atp2a3*'. The neuron-associated microglial signature was selected from the differential expression between granule cell proximal microglia in the old compared to the young mice. We then computed these scores as a function of distance to granule cells either in the cerebellum (CB Granule Glut) or in the hippocampus (DG Glut) in both young (3 months) and old (24

months) mice. Each granule cell identified within 100 μm distance of a microglial cell was identified using kD-tree search in scikit-learn as explained previously.[24] The average cell cycle or neuron-associated microglia score was then calculated at one-micron steps from zero to seventy microns with a sliding twenty-micron window. The mean activation was also subtracted from these ranges so that they are centered around zero.

After establishing a neuron-associated microglial signature, we then performed differential gene expression analysis between young and old microglia that were within thirty microns of granule cells in either the cerebellum or the hippocampus. The differential gene expression between the cells was estimated using the Mann-Whitney-Wilcoxon test and sorted by log fold change from young to old.

Immunofluorescence staining and image analysis: Perfused brains from 3- or 24-month-old mice and fixed in 4% paraformaldehyde for 24 h at 4°C. After fixation, brains were cryoprotected in 30% sucrose at 4°C until fully infiltrated and then embedded. Brains were cut into 40-μm free-floating sections using a microtome. At least three paired brain sections per experiment were used for immunostaining. The sections were first washed and permeabilized in 0.1% Triton X-100 in PBS (PBST), then blocked with 5% normal donkey serum in PBST for 1 h at room temperature (RT). Sections were incubated overnight at 4°C with primary antibodies in 5% normal donkey serum in PBST: Iba1 (goat, Novus Biologicals #NB100–1028, 1:1000), GABRA6 (rabbit, Synaptic Systems #224603, 1:500; AB_2564653), and Hoechst 33342 (Miltenyi Biotech #130–111-569, 1:10,000). After primary antibody incubation, sections were washed and incubated with appropriate species-specific AlexaFluor secondary antibodies (diluted 1:1000 in 5% normal donkey serum in PBST) for 1 h at RT. Sections were then washed three times in PBST for a total of 30 min, counterstained, and mounted on slides. Immunofluorescence staining was based on published methods and images were captured using a fluorescence microscope with consistent exposure and gain settings across stains and animals.[44]

Images were captured on a Leica Stellaris8 confocal microscope at high magnification and analyzed using ImageJ software (NIH); results were obtained from an average of at least three sections per mouse, with a threshold applied to all images. The threshold function in ImageJ was used to determine the percentage of immunoreactive area of the microglial marker (IBA1) within the granule layer (GABRA6), the region of interest (ROI). Plots were generated using GraphPad Prism (version 10.4.0).

Supplementary Material

Refer to Web version on PubMed Central for supplementary material.

ACKNOWLEDGMENTS

The authors thank the past and present members of the Wyss-Coray lab, Quake lab, Chan Zuckerberg Biohub, and Knight Initiative lab for their feedback, valuable discussions, and support throughout the study. This work was supported by the Larry L. Hillblom Foundation (A.P.T.), the Milky Way Research Foundation (T.W.-C.), the Simons Foundation (T.W.-C.), the D.H. Chen Foundation (T.W.-C.), the Knight Initiative for Brain Resilience (T.W.-C.), NIA R01 grant AG072255 (T.W.-C.), and the Chan Zuckerberg Biohub (S.R.Q.).

REFERENCES

1. Tian YE, Cropley V, Maier AB, Lautenschlager NT, Breakspear M, and Zalesky A (2023). Heterogeneous aging across multiple organ systems and prediction of chronic disease and mortality. Nat. Med. 29, 1221–1231. 10.1038/s41591-023-02296-6. [PubMed: 37024597]
2. Hou Y, Dan X, Babbar M, Wei Y, Hasselbalch SG, Croteau DL, and Bohr VA (2019). Ageing as a risk factor for neurodegenerative disease. Nat. Rev. Neurol. 15, 565–581. 10.1038/s41582-019-0244-7. [PubMed: 31501588]
3. Hahn O, Foltz AG, Atkins M, Kedir B, Moran-Losada P, Guldner IH, Munson C, Kern F, Pálovics R, Lu N, et al. (2023). Atlas of the aging mouse brain reveals white matter as vulnerable foci. Cell 186, 4117–4133.e22. 10.1016/j.cell.2023.07.027. [PubMed: 37591239]
4. Feng X, Guo J, Sigmon HC, Sloan RP, Brickman AM, Provenzano FA, and Small SA; Alzheimer's Disease Neuroimaging Initiative (2020). Brain regions vulnerable and resistant to aging without Alzheimer's disease. PLoS One 15, e0234255. 10.1371/journal.pone.0234255. [PubMed: 32726311]
5. Grabert K, Michoel T, Karavolos MH, Clohisey S, Baillie JK, Stevens MP, Freeman TC, Summers KM, and McColl BW (2016). Microglial brain region-dependent diversity and selective regional sensitivities to aging. Nat. Neurosci. 19, 504–516. 10.1038/nn.4222. [PubMed: 26780511]
6. Soreq L, UK Brain Expression Consortium; North American Brain Expression Consortium; Rose J, Soreq E, Hardy J, Trabzuni D, Cookson MR, Smith C, Ryten M, et al. (2017). Major Shifts in Glial Regional Identity Are a Transcriptional Hallmark of Human Brain Aging. Cell Rep. 18, 557–570. 10.1016/j.celrep.2016.12.011. [PubMed: 28076797]
7. Azevedo FAC, Carvalho LRB, Grinberg LT, Farfel JM, Ferretti REL, Leite REP, Jacob Filho W, Lent R, and Herculano-Houzel S (2009). Equal numbers of neuronal and nonneuronal cells make the human brain an isometrically scaled-up primate brain. J. Comp. Neurol. 513, 532–541. 10.1002/cne.21974. [PubMed: 19226510]
8. Schmahmann JD (2019). The cerebellum and cognition. Neurosci. Lett. 688, 62–75. 10.1016/j.neulet.2018.07.005. [PubMed: 29997061]
9. Wagner MJ, and Luo L (2020). Neocortex-Cerebellum Circuits for Cognitive Processing. Trends Neurosci. 43, 42–54. 10.1016/j.tins.2019.11.002. [PubMed: 31787351]
10. Hampel H, Hardy J, Blennow K, Chen C, Perry G, Kim SH, Villemagne VL, Aisen P, Vendruscolo M, Iwatsubo T, et al. (2021). The Amyloid-β Pathway in Alzheimer's Disease. Mol. Psychiatry 26, 5481–5503. 10.1038/s41380-021-01249-0. [PubMed: 34456336]
11. Gellersen HM, Guell X, and Sami S (2021). Differential vulnerability of the cerebellum in healthy ageing and Alzheimer's disease. Neuroimage. Clin. 30, 102605. 10.1016/j.nicl.2021.102605. [PubMed: 33735787]
12. Lopez G, Magaki SD, Williams CK, Paganini-Hill A, and Vinters HV (2024). Characterization of cerebellar amyloid-β deposits in Alzheimer disease. J. Neuropathol. Exp. Neurol. 83, 72–78. 10.1093/jnen/nlad107. [PubMed: 38114098]
13. Podleśny-Drabiniok A, Marcora E, and Goate AM (2020). Microglial Phagocytosis: A Disease-Associated Process Emerging from Alzheimer's Disease Genetics. Trends Neurosci. 43, 965–979. 10.1016/j.tins.2020.10.002. [PubMed: 33127097]
14. Tsai AP, Dong C, Lin PBC, Messenger EJ, Casali BT, Moutinho M, Liu Y, Oblak AL, Lamb BT, Landreth GE, et al. (2022). PLCG2 is associated with the inflammatory response and is induced by amyloid plaques in Alzheimer's disease. Genome Med. 14, 17. 10.1186/s13073-022-01022-0. [PubMed: 35180881]
15. Ayata P, Badimon A, Strasburger HJ, Duff MK, Montgomery SE, Loh YHE, Ebert A, Pimenova AA, Ramirez BR, Chan AT, et al. (2018). Epigenetic regulation of brain region-specific microglia clearance activity. Nat. Neurosci. 21, 1049–1060. 10.1038/s41593-018-0192-3. [PubMed: 30038282]
16. Morterá P, and Herculano-Houzel S (2012). Age-related neuronal loss in the rat brain starts at the end of adolescence. Front. Neuroanat. 6, 45. 10.3389/fnana.2012.00045. [PubMed: 23112765]

17. Pembroke WG, Hartl CL, and Geschwind DH (2021). Evolutionary conservation and divergence of the human brain transcriptome. Genome Biol. 22, 52. 10.1186/s13059-020-02257-z. [PubMed: 33514394]

18. Kozareva V, Martin C, Osorno T, Rudolph S, Guo C, Vanderburg C, Nadaf N, Regev A, Regehr WG, and Macosko E (2021). A transcriptomic atlas of mouse cerebellar cortex comprehensively defines cell types. Nature 598, 214–219. 10.1038/s41586-021-03220-z. [PubMed: 34616064]

19. Tsai AP, Dong C, Lin PBC, Oblak AL, Viana Di Prisco G, Wang N, Hajicek N, Carr AJ, Lendy EK, Hahn O, et al. (2023). Genetic variants of phospholipase C-γ2 alter the phenotype and function of microglia and confer differential risk for Alzheimer's disease. Immunity 56, 2121–2136.e6. 10.1016/j.immuni.2023.08.008. [PubMed: 37659412]

20. Haney MS, Pálovics R, Munson CN, Long C, Johansson PK, Yip O, Dong W, Rawat E, West E, Schlachetzki JCM, et al. (2024). APOE4/4 is linked to damaging lipid droplets in Alzheimer's disease microglia. Nature 628, 154–161. 10.1038/s41586-024-07185-7. [PubMed: 38480892]

21. de Magalhães JP, Abidi Z, Dos Santos GA, Avelar RA, Barardo D, Chatsirisupachai K, Clark P, De-Souza EA, Johnson EJ, Lopes I, et al. (2024). Human Ageing Genomic Resources: updates on key databases in ageing research. Nucleic Acids Res. 52, D900–D908. 10.1093/nar/gkad927. [PubMed: 37933854]

22. Hu Y, Fryatt GL, Ghorbani M, Obst J, Menassa DA, Martin-Estebane M, Muntslag TAO, Olmos-Alonso A, Guerrero-Carrasco M, Thomas D, et al. (2021). Replicative senescence dictates the emergence of disease-associated microglia and contributes to Aβ pathology. Cell Rep. 35, 109228. 10.1016/j.celrep.2021.109228. [PubMed: 34107254]

23. Keren-Shaul H, Spinrad A, Weiner A, Matcovitch-Natan O, Dvir-Szternfeld R, Ulland TK, David E, Baruch K, Lara-Astaiso D, Toth B, et al. (2017). A Unique Microglia Type Associated with Restricting Development of Alzheimer's Disease. Cell 169, 1276–1290.e17. 10.1016/j.cell.2017.05.018. [PubMed: 28602351]

24. Allen WE, Blosser TR, Sullivan ZA, Dulac C, and Zhuang X (2023). Molecular and spatial signatures of mouse brain aging at single-cell resolution. Cell 186, 194–208.e18. 10.1016/j.cell.2022.12.010. [PubMed: 36580914]

25. Yao Z, van Velthoven CTJ, Kunst M, Zhang M, McMillen D, Lee C, Jung W, Goldy J, Abdelhak A, Aitken M, et al. (2023). A high-resolution transcriptomic and spatial atlas of cell types in the whole mouse brain. Nature 624, 317–332. 10.1038/s41586-023-06812-z. [PubMed: 38092916]

26. Oh HSH, Rutledge J, Nachun D, Pálovics R, Abiose O, Moran-Losada P, Channappa D, Urey DY, Kim K, Sung YJ, et al. (2023). Organ aging signatures in the plasma proteome track health and disease. Nature 624, 164–172. 10.1038/s41586-023-06802-1. [PubMed: 38057571]

27. Kebschull JM, Richman EB, Ringach N, Friedmann D, Albarran E, Kolluru SS, Jones RC, Allen WE, Wang Y, Cho SW, et al. (2020). Cerebellar nuclei evolved by repeatedly duplicating a conserved cell-type set. Science 370, eabd5059. 10.1126/science.abd5059. [PubMed: 33335034]

28. Li X, Li Y, Jin Y, Zhang Y, Wu J, Xu Z, Huang Y, Cai L, Gao S, Liu T, et al. (2023). Transcriptional and epigenetic decoding of the microglial aging process. Nat. Aging 3, 1288–1311. 10.1038/s43587-023-00479-x. [PubMed: 37697166]

29. Moutinho M, Puntambekar SS, Tsai AP, Coronel I, Lin PB, Casali BT, Martinez P, Oblak AL, Lasagna-Reeves CA, Lamb BT, and Landreth GE (2022). The niacin receptor HCAR2 modulates microglial response and limits disease progression in a mouse model of Alzheimer's disease. Sci. Transl. Med. 14, eabl7634. 10.1126/scitranslmed.abl7634. [PubMed: 35320002]

30. Marschallinger J, Iram T, Zardeneta M, Lee SE, Lehallier B, Haney MS, Pluvinage JV, Mathur V, Hahn O, Morgens DW, et al. (2020). Lipid-droplet-accumulating microglia represent a dysfunctional and proinflammatory state in the aging brain. Nat. Neurosci. 23, 194–208. 10.1038/s41593-019-0566-1. [PubMed: 31959936]

31. Jaffe AE, Hoeppner DJ, Saito T, Blanpain L, Ukaigwe J, Burke EE, Collado-Torres L, Tao R, Tajinda K, Maynard KR, et al. (2020). Profiling gene expression in the human dentate gyrus granule cell layer reveals insights into schizophrenia and its genetic risk. Nat. Neurosci. 23, 510–519. 10.1038/s41593-020-0604-z. [PubMed: 32203495]

32. Chawla MK, and Barnes CA (2007). Hippocampal granule cells in normal aging: insights from electrophysiological and functional imaging experiments. Prog. Brain Res. 163, 661–678. 10.1016/s0079-6123(07)63036-2. [PubMed: 17765744]

33. Iskusnykh IY, Zakharova AA, Kryl'skii ED, and Popova TN (2024). Aging, Neurodegenerative Disorders, and Cerebellum. Int. J. Mol. Sci. 25, 1018. 10.3390/ijms25021018. [PubMed: 38256091]
34. Miyata M, Kishimoto Y, Tanaka M, Hashimoto K, Hirashima N, Murata Y, Kano M, and Takagishi Y (2011). A role for myosin Va in cerebellar plasticity and motor learning: a possible mechanism underlying neurological disorder in myosin Va disease. J. Neurosci. 31, 6067–6078. 10.1523/jneurosci.5651-10.2011. [PubMed: 21508232]
35. DeWard AD, Eisenmann KM, Matheson SF, and Alberts AS (2010). The role of formins in human disease. Biochim. Biophys. Acta 1803, 226–233. 10.1016/j.bbamcr.2009.11.006. [PubMed: 19941910]
36. Sabogal-Guáqueta AM, Marmolejo-Garza A, Trombetta-Lima M, Oun A, Hunneman J, Chen T, Koistinaho J, Lehtonen S, Kortholt A, Wolters JC, et al. (2023). Species-specific metabolic reprogramming in human and mouse microglia during inflammatory pathway induction. Nat. Commun. 14, 6454. 10.1038/s41467-023-42096-7. [PubMed: 37833292]
37. Shulman JM, Imboywa S, Giagtzoglou N, Powers MP, Hu Y, Devenport D, Chipendo P, Chibnik LB, Diamond A, Perrimon N, et al. (2014). Functional screening in Drosophila identifies Alzheimer's disease susceptibility genes and implicates Tau-mediated mechanisms. Hum. Mol. Genet. 23, 870–877. 10.1093/hmg/ddt478. [PubMed: 24067533]
38. Lu N, Moran-Losada P, Hahn O, Saksena A, Tapp E, Chadarevian JP, Dong W, Shi SM, Shuken SR, Guldner I, et al. (2024). Circulatory proteins shape microglia state and boost phagocytosis. bioRxiv. 10.1101/2024.09.30.615861.
39. Wu AR, Neff NF, Kalisky T, Dalerba P, Treutlein B, Rothenberg ME, Mburu FM, Mantalas GL, Sim S, Clarke MF, and Quake SR (2014). Quantitative assessment of single-cell RNA-sequencing methods. Nat. Methods 11, 41–46. 10.1038/nmeth.2694. [PubMed: 24141493]
40. De Miguel Z, Khoury N, Betley MJ, Lehallier B, Willoughby D, Olsson N, Yang AC, Hahn O, Lu N, Vest RT, et al. (2021). Exercise plasma boosts memory and dampens brain inflammation via clusterin. Nature 600, 494–499. 10.1038/s41586-021-04183-x. [PubMed: 34880498]
41. Krasemann S, Madore C, Cialic R, Baufeld C, Calcagno N, El Fatimy R, Beckers L, O'Loughlin E, Xu Y, Fanek Z, et al. (2017). The TREM2-APOE Pathway Drives the Transcriptional Phenotype of Dysfunctional Microglia in Neurodegenerative Diseases. Immunity 47, 566–581.e9. 10.1016/j.immuni.2017.08.008. [PubMed: 28930663]
42. Henze DE, Tsai AP, Wyss-Coray T, and Quake SR (2025). Simultaneous analysis of single-cell gene expression and morphology provides new insight into how microglia change with age. bioRxiv. 10.1101/2025.02.28.640888.
43. Zhang M, Pan X, Jung W, Halpern AR, Eichhorn SW, Lei Z, Cohen L, Smith KA, Tasic B, Yao Z, et al. (2023). Molecularly defined and spatially resolved cell atlas of the whole mouse brain. Nature 624, 343–354. 10.1038/s41586-023-06808-9. [PubMed: 38092912]
44. Tsai AP, Lin PBC, Dong C, Moutinho M, Casali BT, Liu Y, Lamb BT, Landreth GE, Oblak AL, and Nho K (2021). INPP5D expression is associated with risk for Alzheimer's disease and induced by plaque-associated microglia. Neurobiol. Dis. 153, 105303. 10.1016/j.nbd.2021.105303. [PubMed: 33631273]

Highlights

- Aging induces distinct transcriptional changes in cerebellar microglia
- Multi-omics analyses reveal molecular and spatial adaptations in cerebellar microglia
- Microglia-neuron proximity increases in the aged cerebellum
- Neuron-associated microglia show a higher neuroprotective signature

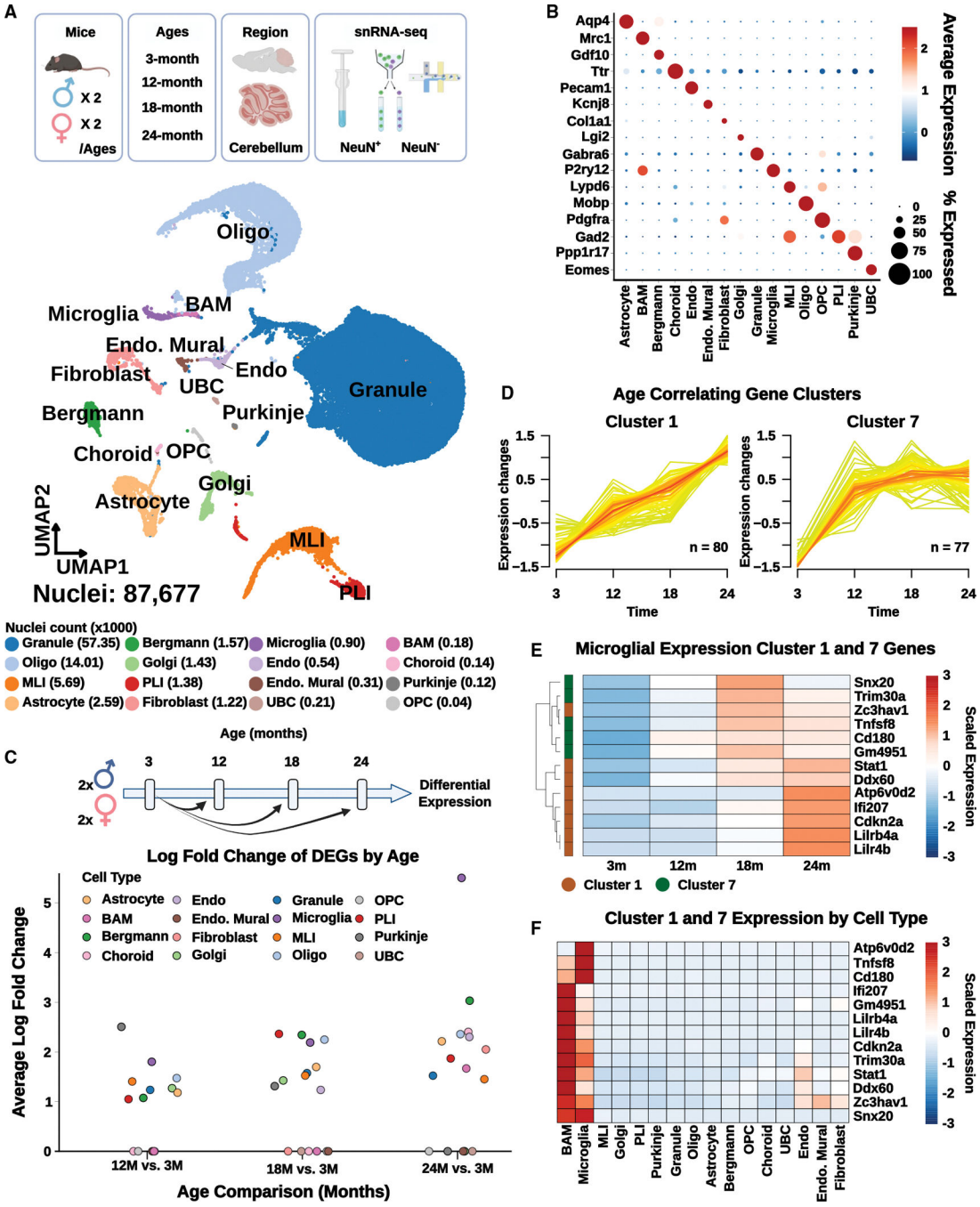

Figure 1. Distinct transcriptional aging patterns in cerebellar cells

(A) Schematic representation of the experimental workflow for isolating and enriching glial nuclei from cerebellar tissue of 3-, 12-, 18-, and 24-month-old mice, followed by single-nucleus RNA sequencing (snRNA-seq). A uniform manifold approximation and projection (UMAP) visualization of 87,677 nuclei, colored by cell type, is shown, with the corresponding counts listed.

(B) Dot plot of scaled expression levels for selected marker genes used to define cell types.

(C) Scatterplot illustrating the average fold change of the top ten differentially expressed genes (DEGs) for each cell type, with comparisons made between each age group and 3-month-old mice. Dots are color coded to represent cell types.
(D) Age-dependent cerebellar gene expression changes are grouped into nine distinct clusters, with clusters 1 and 7 showing progressively increasing expression levels with age.
(E and F) Heatmaps showing the expression levels of top genes from clusters 1 and 7 across four age groups (E) and among 15 cell types (F).

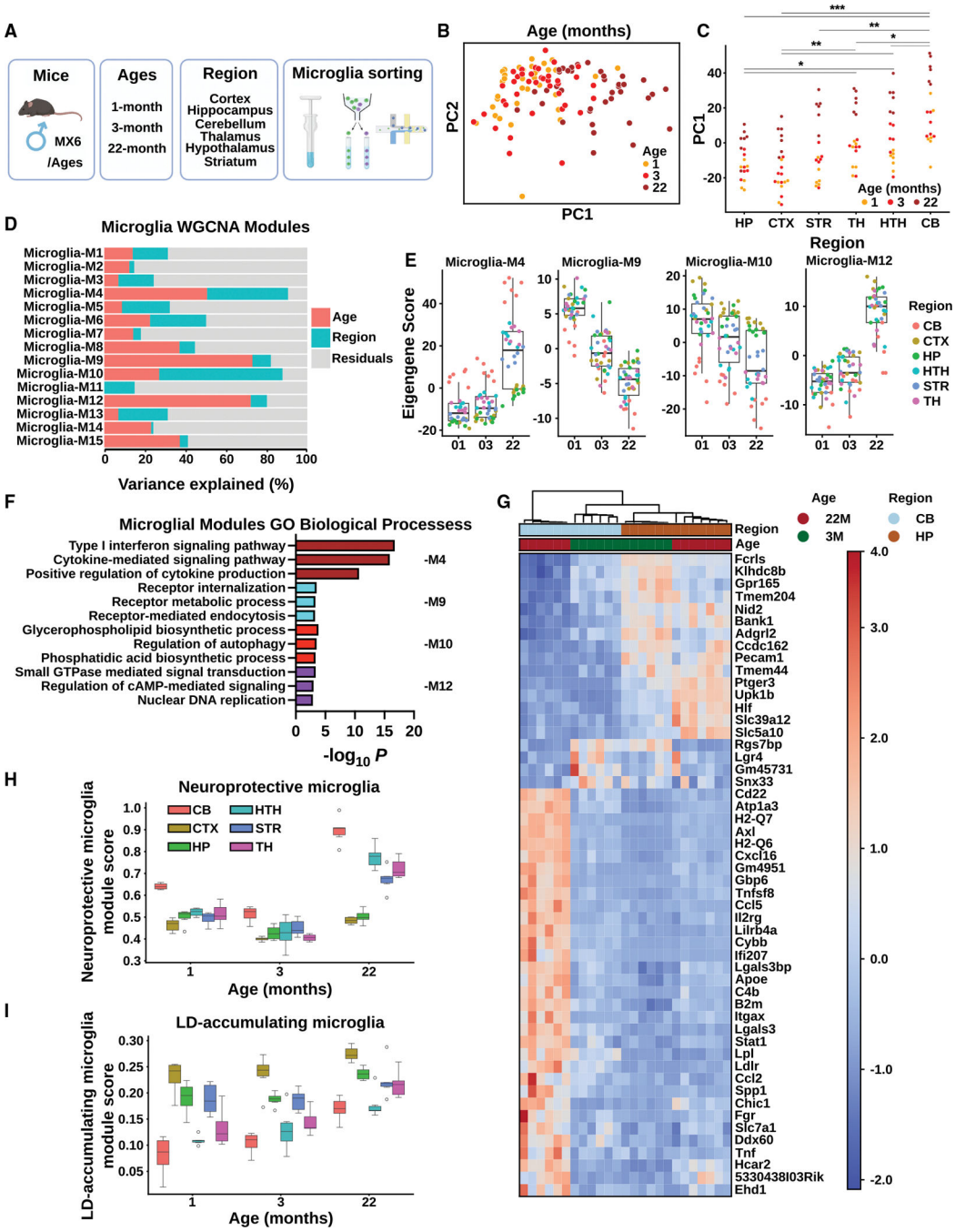

Figure 2. Regional and age-associated transcriptional signatures of microglia

(A) Schematic of the experimental workflow for isolating microglia from six brain regions, the cerebellum (CB), cortex (CTX), hippocampus (HP), hypothalamus (HTH), striatum (STR), and thalamus (TH), from 1-, 3-, and 22-month-old male mice.

(B) Principal-component analysis (PCA) plot showing microglial transcriptional profiles differences across age groups and brain regions.

(C) Line plot of PC1 values across six brain regions, illustrating age-related transcriptional changes and unique aging trajectories of microglia. Pairwise regional differences were

assessed using the Wilcoxon rank-sum test with Benjamini-Hochberg correction (*$p < 0.05$, **$p < 0.01$, and ***$p < 0.001$).

(D) Bar chart depicting the percentage of variance explained by 15 microglial co-expression modules identified using weighted gene co-expression network analysis (WGCNA), highlighting the contributions of age and brain region.

(E) Boxplots of eigengene scores for microglial modules M4, M9, M10, and M12, demonstrating region- and age-specific expression patterns across three age groups.

(F) Bar chart of top enriched Gene Ontology (GO) biological processes for genes within microglial modules M4, M9, M10, and M12.

(G) Heatmap showing top differentially expressed genes (DEGs) across two comparisons: 22-month-old versus 3-month-old mice and cerebellum versus hippocampus.

(H and I) Boxplot showing the expression of the neuroprotective microglial signature (H) and the lipid-droplet (LD)-accumulating microglial signature (I), across three age groups and six brain regions.

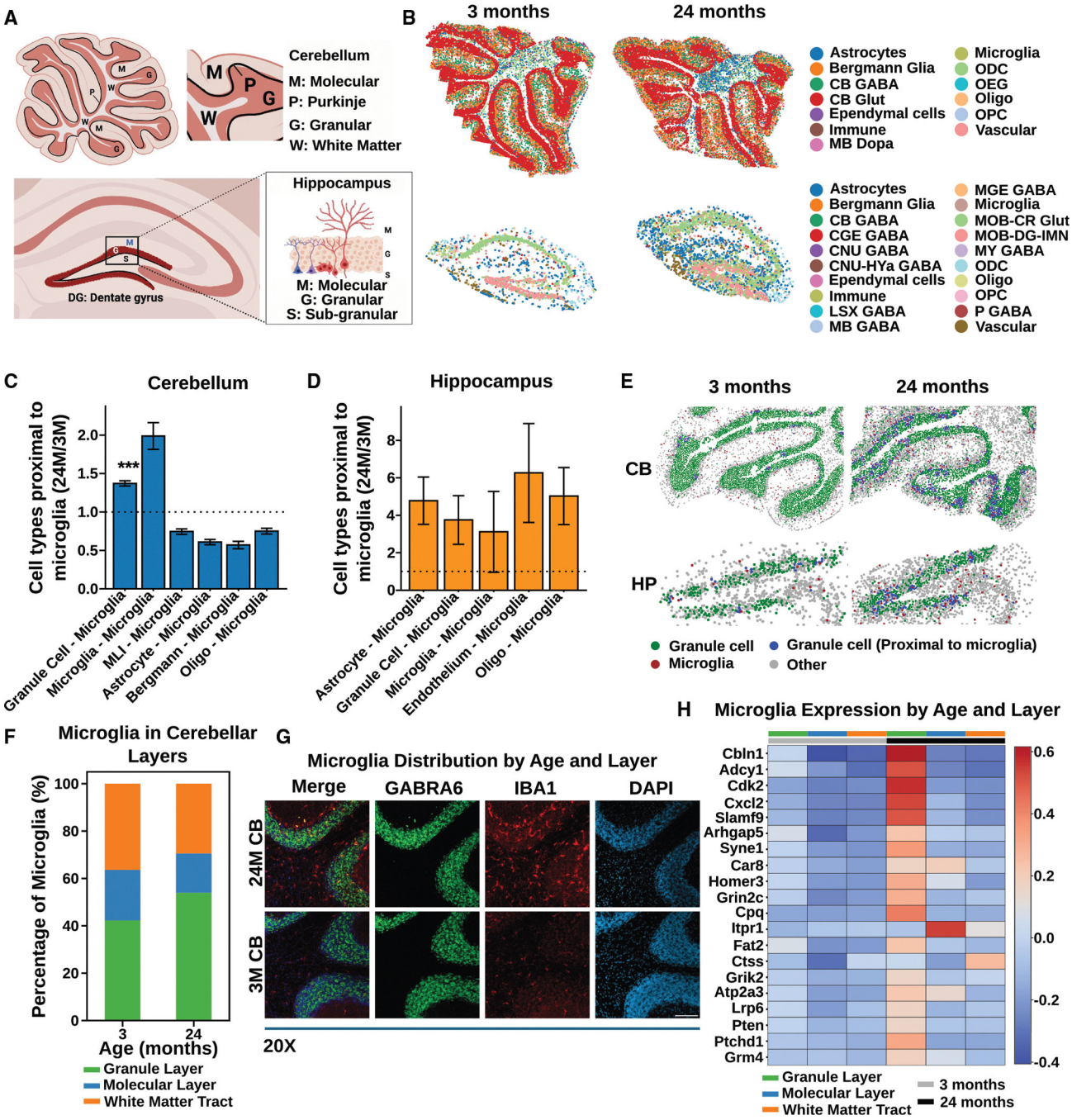

Figure 3. Increased microglial proximity to granule cells defines the aged cerebellum

(A) Schematic overview of the cellular layers of mouse cerebellum and hippocampus.

(B) MERFISH imaging of cerebellum and hippocampus from 3- and 24-month-old mice, colored by major cell types.

(C and D) Bar plot showing the changes in microglial proximity to cerebellar (C) and hippocampal (D) cell types in aged versus young mice. Proximity ratios (24 months old/3 months old) for cell-microglia contacts were computed relative to permutation-based null distributions (1,000 iterations), with standard errors estimated by the delta method. Two-

tailed z-tests were performed against the null expectation, and *p* values were corrected using the Benjamini-Hochberg false discovery rate (FDR) method. Bars represent the mean ± SEM. *$p < 0.05$ and *$p < 0.05$.

(E) MERFISH imaging highlighting microglia (maroon), granule cells distant from microglia (green), granule cells near microglia (blue), and other cells (gray) in the cerebellum and hippocampus of 3- and 24-month-old mice.

(F) Stacked bar plot showing the proportion of microglia within the molecular layer, granule layer, and white matter area of the cerebellum in 3- and 24-month-old mice.

(G) Representative images of cerebellum from 3-month-old and 24-month-old mice, stained with GABRA6 to label granule cells (green), IBA1 to label microglia (red), and DAPI to label nuclei (blue). Scale bar: 100 μm.

(H) Heatmap showing the top differentially expressed genes in microglia from the granule layer (green) compared to the molecular layer (blue) and white matter area (orange) in the aged cerebellum (black).

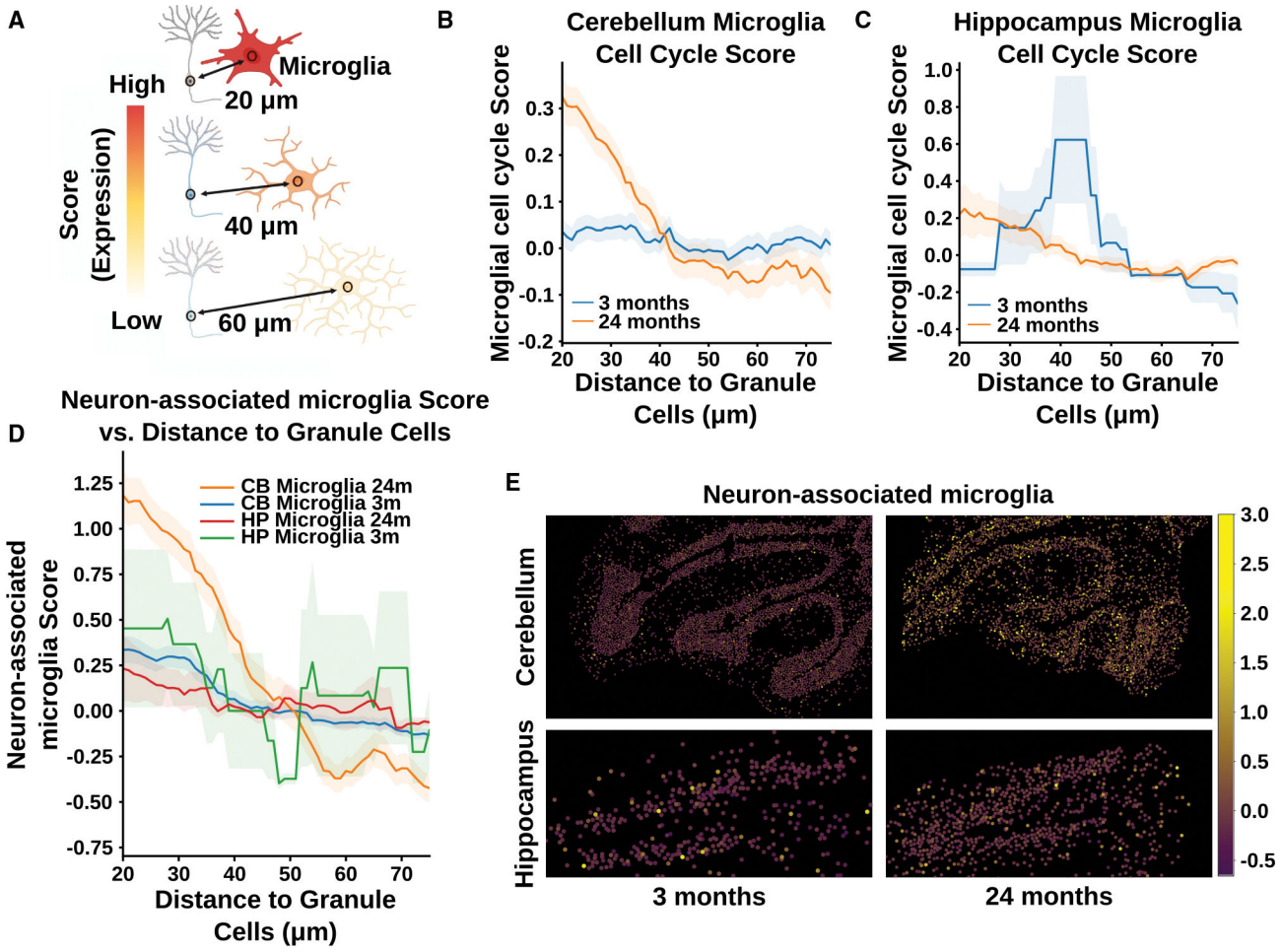

Figure 4. Cerebellar microglial states are associated with spatial proximity to granule cells

(A) Schematic illustrating the experimental workflow to examine the spatial distribution of microglial signatures and their proximity-dependent influence relative to granule cells.

(B and C) The expression of microglial cell cycle signature at varying distances from granule cells in the cerebellum (B) and hippocampal dentate gyrus (C) of 3- (blue) or 24- (orange) month-old mice.

(D) Line chart showing the expression of neuron-associated microglial signature at different distances from granule cells in the cerebellum and hippocampal dentate gyrus across age groups.

(E) MERFISH images showing expression of neuron-associated microglial signature in the cerebellum and hippocampus of young (3-month-old) and aged (24-month-old) mice.

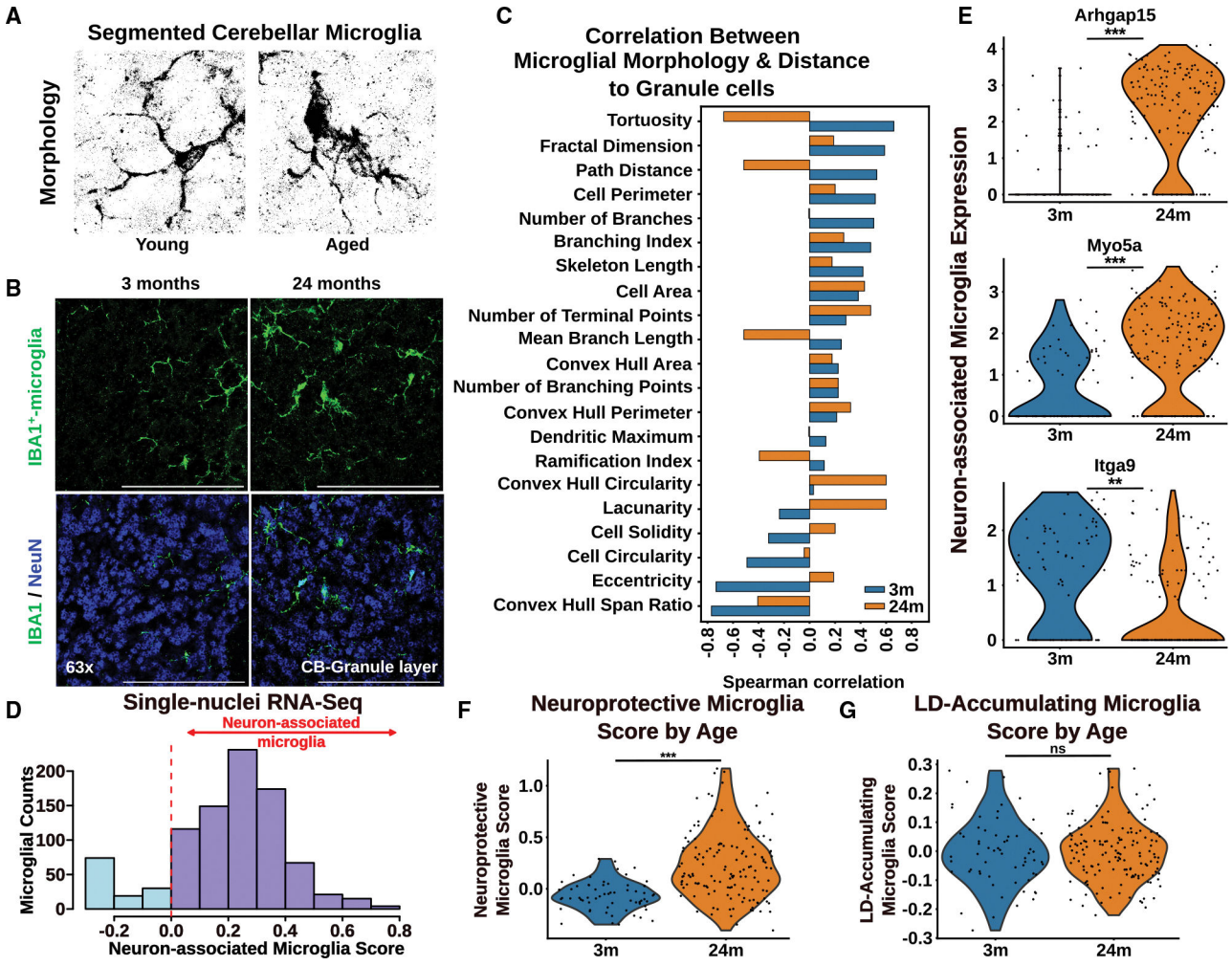

Figure 5. Age-associated adaptations in neuron-associated microglia

(A) Schematic representation illustrating age-related changes in microglial morphology in cerebellum.

(B) Immunofluorescence staining for IBA1-positive (green) and NeuN-positive cells in the cerebellar granule layer at 3 and 24 months. Scale bar: 100 μm.

(C) Spearman correlation coefficients between microglial morphological features and distance to granule cells in young (blue) and aged (orange) cerebella.

(D) Classification of cerebellar microglia from single-nucleus RNA-seq based on expression of neuron-associated microglial signature, with cells showing positive scores classified as neuron-associated microglia.

(E) Expression of top differentially expressed genes (*Arhgap15*, *Myo5a*, and *Itga9*) in neuron-associated microglia from 3- and 24-month-old mice.

(F) Expression of neuroprotective microglial signature in neuron-associated microglia, showing a significant increase in aged cerebellum ($p < 0.05$).

(G) Expression of lipid-droplet (LD)-accumulating microglial signature in neuron-associated microglia, showing no significant change with age. Wilcoxon rank-sum test comparing

3-month-old versus 24-month-old neuron-associated microglia. *$p < 0.05$ and ns, not significant.

KEY RESOURCES TABLE

REAGENT or RESOURCE	SOURCE	IDENTIFIER
Antibodies and Reagents		
anti-CD16/CD32 Fc block	BD Biosciences	Cat#553142; RRID: AB_394656
IBA1	Novus Biologicals	Cat#NB100-1028; RRID:AB_521594
NeuN	Abcam	#ab190565; RRID:AB_2732785
GABRA6	Synaptic Systems	Cat#224603; RRID:AB_2619945
UltraPure BSA	Thermo	Cat#AM2618
Nuclei EZ Prep Kit	Sigma-Aldrich	Cat#Nuc101-1KT
Recombinant RNase Inhibitor	Takara	Cat#2313B
Deposited data		
Sequencing data	GEO	GSE290806
Experimental models: Organisms/strains		
Mouse	C57BL/6J	**RRID:IMSR_JAX:000664**
Software and algorithms		
Prism	GraphPad	version 10.4.0